EVREST Project Report:
Remote Sensing Database Report

Project Funding: Fundação para a Ciência e a Tecnologia (FCT)

Scientific Domain: Marine Sciences and Earth Sciences - Estuarine Coastal and Littoral Systems

Project reference: PTDC/MAREST/1031/2014

Report Title	Remote Sensing Database Report
Reporting Period	01/06/2017 to 31/05/2017
Authors	Katerina Kombiadou & Ana Matias
Delivery Date	31/05/2017
Related Task	Task 1: Data collection and GIS integration
Participants	Katerina Kombiadou, Gustavo Vieira, Alkisti Pliatsika, Ana Matias, Óscar Ferreira & Carlos Loureiro

Funded by

Project reference: PTDC/MAR-EST/1031/2014

TABLE OF CONTENTS

TABLE OF FIGURES

INDEX OF TABLES

1. INTRODUCTION

1.1 General

The present report covers the activities performed in the framework of 'Task 1: Data collection and GIS integration' regarding the formulation of a geodatabase for the morphological evolution of Ria Formosa with what concerns raster datasets. The following sections include an analysis of the types and characteristics of the available data and the process followed by georeferencing and mosaicking of the raster datasets collected.

1.2 Study sites

The analysis refers to the four study sites selected in the project, as representative of the four main geomorphological environments considered in the project, namely:

- ✓ Barreta Island: dunes
- ✓ Culatra Island: salt marshes
- ✓ Tavira Island: pristine stable zones
- ✓ Cabanas Island/Cacela Peninsula: sandy barrier islands

The location of the sites is presented in figure 1.

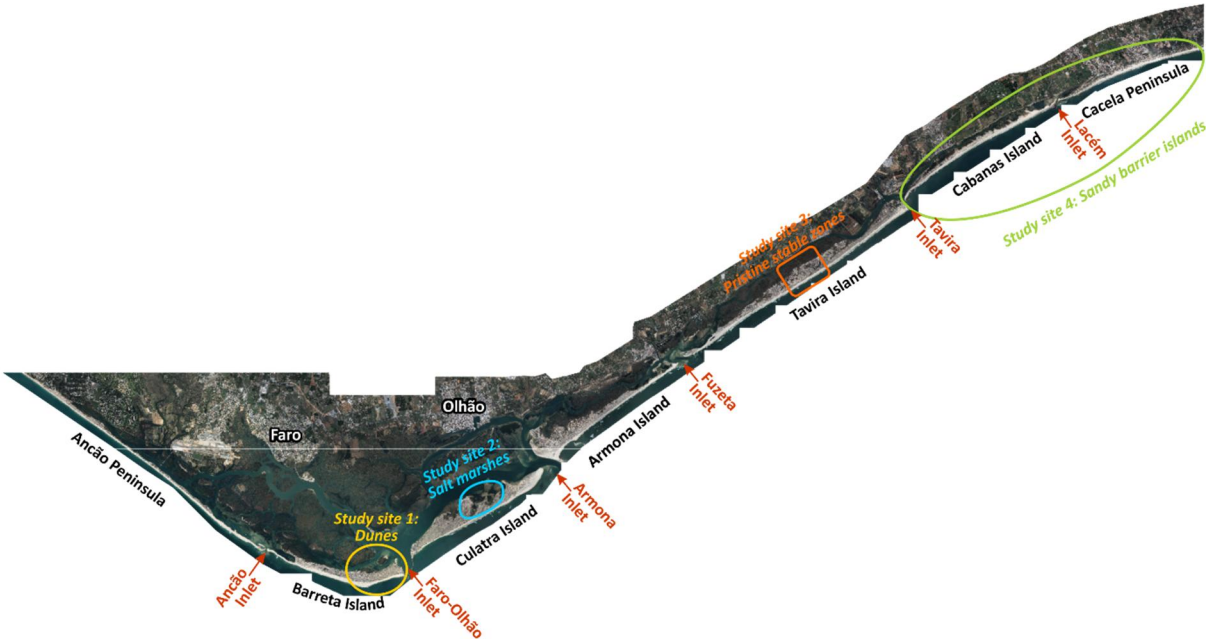

Figure 1: Location of the 4 EVREST study sites in the Ria Formosa system

1.3 Software

The GIS was built using the ESRI ArcMap 10.1 software; necessary program extensions were activated (3D, Spatial, and Geostatistical Analyst and Data Interoperability).

2. AVAILABLE DATA

The data collected for the development of the EVREST GIS platform include aerial photographs, ortho-photographs and high-resolution, LIDAR (Light Detection and Ranging) -based, terrain models, with the most recent data from 2014 and the oldest from 1947. Table 1 includes a list of the available aerial or ortho- photographs (raster data) and LIDAR data collected and processed in the framework of the project, along with the main characteristics and the coverage of the flight in each of the four EVREST study cases.

Table 1: List of available raster and LIDAR data, photography type (AP: Aerial Photos; OP: OrthoPhotos), scale, bands (1: BW, 3: RGB, 4: RGB+Infrared) and flight coverage of the four study sites are provided.

Year	Type	Scale/ Resolution	Bands	Study Site Coverage			
				Barreta	Culatra	Tavira	Cabanas /Cacela
1947	AP	unknown	1	full	full	full	full
1952	AP	1:20000	1	full	full	full	full
1958	AP	1:26000	1	full	full	full	full
1969	AP	1:25000	1	none	partial	full	full
1972	AP	1:6000	1	full	full	full	partial
1976	AP	1:30000	1	full	full	full	full
1980	AP	unknown	1	full	full	full	full
1985	AP	1:15000	1	full	full	full	full
1986	AP	1:8000	3	full	full	full	full
1989	AP	1:10000	1	partial	none	full	full
1989	AP	1:8000	3	full	full	full	full
1996	AP	1:8000	3	full	full	full	full
1999	AP	1:8000	3	full	full	full	none
2000	AP	1:8000	3	full	full	full	none
2001	AP	1:8000	3	full	full	full	full
2002	OP	70cm	3	full	full	full	full
2005	OP	70cm	3	full	full	full	full
2008	OP	15cm	4	full	full	full	full
2009	OP	10cm	3	full	full	none	none
2009	LIDAR	10cm	1	full	full	none	none
2011	LIDAR	10cm	1	full	full	full	full
2014	OP	15cm	4	full	full	full	full

3. Processing of Raster Images

3.1 General Remarks

Digital orthophotography refers to computer-rectified (camera tilt, relief and lens distortion) aerial photographs that include true geographic information. Therefore, the available orthophotography are ready-to-use with no need for further rectification. On the other hand, aerial photography are unprocessed, raster images, with no geographic information linked to it, which need to be georeferenced.

The aerial photos georeferencing process is performed 'backwards' in time, going from the most recent to the oldest photographs. The orthophotography of 2002 was used as the basis for the georeferencing process, as it is the oldest available orthorectified map of the Ria Formosa. Thus, using the 2002 orthophotography, the aerial photographs of the directly previous year (2001) were georeferenced (the process is analysed further down). In turn, the georeferenced photos of 2001 were used as a basis for the 2000 flight and so on. Generally, the basis for the georeferencing of each flight is the directly posterior, available, flight. At the same time, all available georeferenced datasets were used to clarify doubts regarding morphological evolution and to assure the suitability of the selected control points.

3.2 Georeferencing of aerial photography

3.2.1 The raster georeferencing process

The process of georeferencing each aerial photograph incudes overlaying the images (base-map and the raster layer to be georeferenced; figure 2a) and assigning a set of *links* (Figure 2b) that relate the location of a control point in the raster image to the location of the same point in the georeferenced base-map. Thus, adding a list of carefully selected control points, a transformation table (*link table*) is gradually filled in (Figure 2c) that is used for the rectification of the raster image. The residual error for each link is noted on the link table, along with the total RMS error that depends on the transformation method selected (shift, 1^{st}, 2^{nd} or 3^{rd} order transformation, adjust, spline and projective transformation). For the transformation to be applied in the raster, the user needs update the georeferencing at the end of the process.

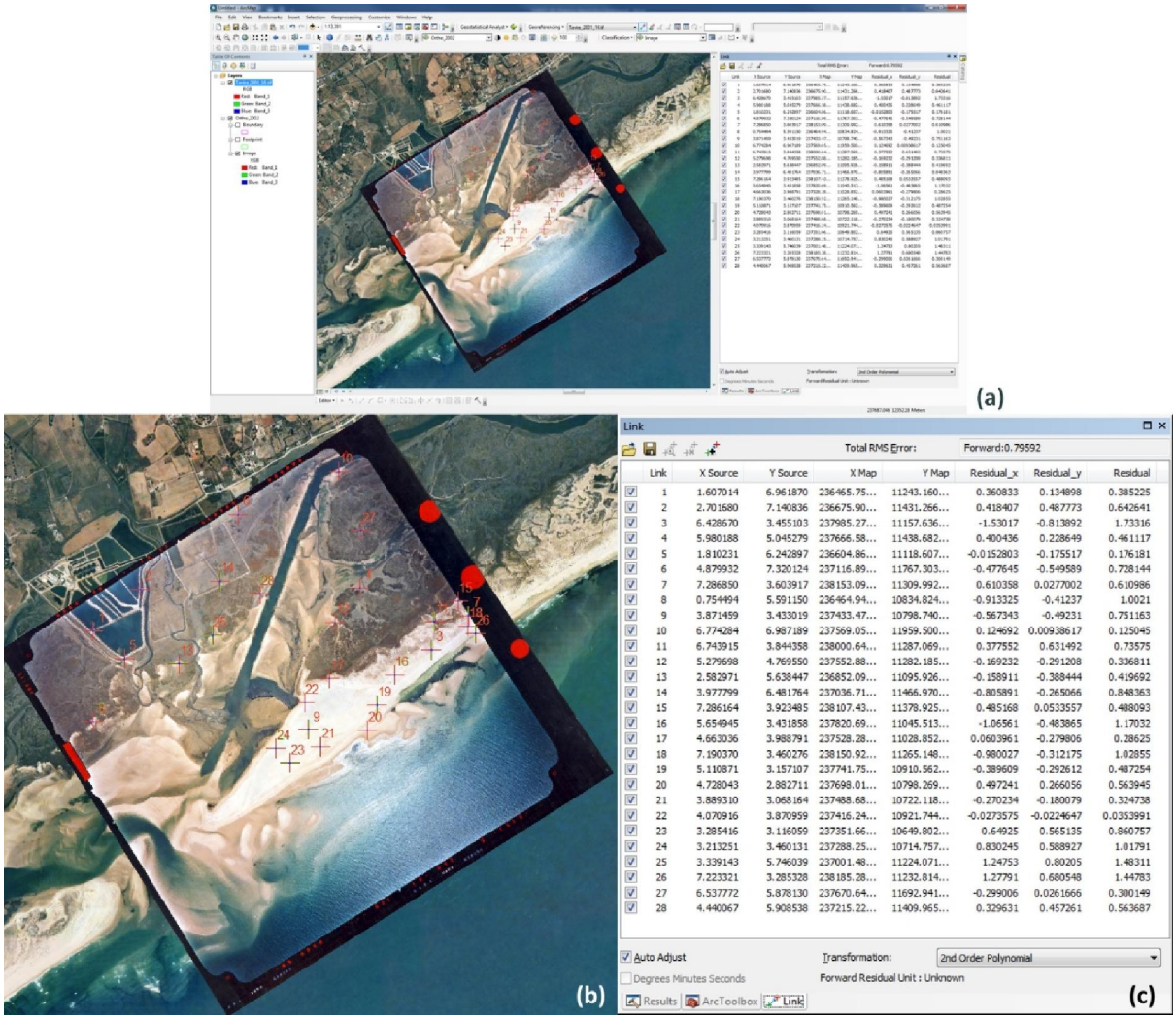

Figure 2: Example of georeferencing aerial photo (a); the location of the selected *links* and the related *link table* are also shown in the zoomed bottom panels (b and c, respectively)

3.2.2 Sources of error and correction

In contrast to orthophotographs that are rectified and accurate vertical imagery, vertical aerial photographs are subject to inherent errors related to distortion and displacement. Distortion in aerial photography is defined as any shift in the position of an image on a photograph that alters the perspective characteristics of the image and displacement is any shift in the position of an image on a photograph that does not alter the perspective characteristics of the photograph (Paine & Kiser, 2012). The principal factors causing distortions to aerial photography include:

- Camera tilt
- Camera lens distortion
- Terrain and Relief displacements

The **camera tilt** refers to the error introduced due to slope in the x and/or y axis of the aircraft (and camera) at the time of the exposure; this causes the isocenter of the photo (point between Nadir and the principal point of the photo) to deviate radially from the principal point (Figure 3). The resultant displacement increases proportionally with tilt.

The **lens distortion** is larger near the edges of the photograph and changes true distances of objects from the principal point. Contemporary, high-quality lenses present minimal distortion, but the error can be significant in the older flights.

Terrain and relief distortions refer to the errors introduced by objects of different height/elevation (i.e. buildings, orography, etc.). Areas of higher elevation are closer to the camera during exposure and, therefore, appear larger, while the top part of tall objects appear displaced (Figure 4). The displacement increases with the elevation height.

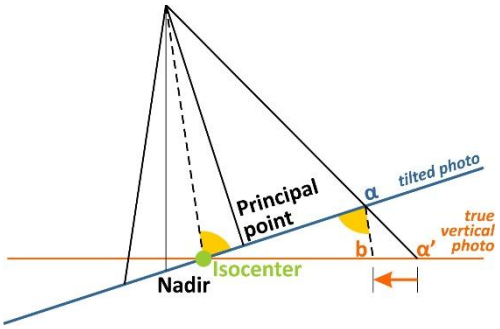

Figure 3: Error due to camera tilt.

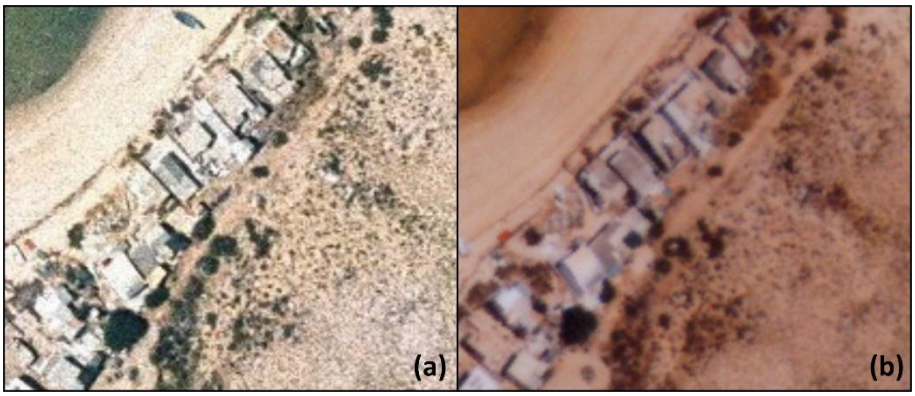

Figure 4: Relief displacement in the case of buildings, as can be observed comparing the orthophotograph of 2002 (a) with the aerial photograph of 2001 (b)

Simple transformation methods, like shift and 1st order, are insufficient to correct these distortions. It was, therefore, necessary to use **higher order transformations** in the georeferencing process. In most cases, and especially for recent flights, 2nd order transformation is selected with **an average number of 30, carefully selected, control points** per photograph. The **total RMS error was kept under 1.0m**.

To minimize the impact of tilt, ground, or near-ground control points were used, like bushes, crossroads or clearly distinguishable soil features, avoiding the use of buildings and tall structures as much as possible. However, in cases of strong and rapidly changing environments, like the Ancão Peninsula, where intense human occupation and activities induced changes to the topographic and natural features, even within the period of one year, that made it very difficult to distinguish reliable control points. In these cases, it was necessary to utilize such points as well. It is noted that, in such cases, the points selected were as near to the ground as possible (i.e. actual position of base corners for buildings or structures), in order to minimize the impact of relief displacement. Furthermore, and especially since higher order transformation was selected, the distribution of the points on the photograph was selected such so as to cover the entire photograph and, at the same time, with increased density in the areas where correction is most important (islands).

3.2.3 Assessment of residual and accumulated error related to georeferencing

Table 2 includes a list of the residual RMS error averaged for all the aerial photographs of each flight and the corresponding values of standard deviation and the total number of photos included in each flight. In general, the error is of the order of 1.0m, which is considered acceptable for the purposes of the project. Most recent flights are high-resolution, which allowed maintaining the RMS error in even lower values (~0.8m).

Table 2: Georeferencing average RMS error, corresponding standard deviation and sample sizes.

Year	Average RMSE [m]	Standard deviation [m]	Sample size [photos]
1947	1.62	0.59	9
1952	1.07	0.64	19
1958	1.10	0.77	12
1969	1.08	0.64	14
1972	0.84	0.55	58
1976	1.13	1.63	19
1980	0.97	1.89	28
1985	1.21	1.59	22
1986	0.65	0.35	38
1989 (BW)	0.99	0.95	48
1989	0.69	0.19	63
1996	0.82	1.01	80
1999	0.58	0.17	56
2000	0.70	0.57	51
2001	0.62	0.20	76

In some cases, and especially in the vicinity of highly energetic and/or migrating inlets, like Ancão and Lacém, finding accurate and reliable control points was very difficult, since entire stretches of the island were newly formed (i.e. near Ancão Inlet in 1972; **Figure 5**). Georeferencing of such problematic areas was performed in both directions along the island (**Figure 5**), so that previously georeferenced photographs of the same flight were utilised to find reliable control points and to gradually cover the newly formed area.

In cases where reliable control points where concentrated on one of the two sides of the aerial photo (i.e. the other falls on the 'problematic' zone), 1st order transformation was used, in order to avoid introducing uncontrollable error and distortions to the photo. This caused the RMS error to increase over the desired levels of 1m, due to the inability of linear transformation to correct distortions in the aerial photo. However, the alternative to try to correct these errors using higher order approximations, without reliable and well-distributed control points, would introduce significantly higher error that would be transferred, magnified, to anterior flights during georeferencing.

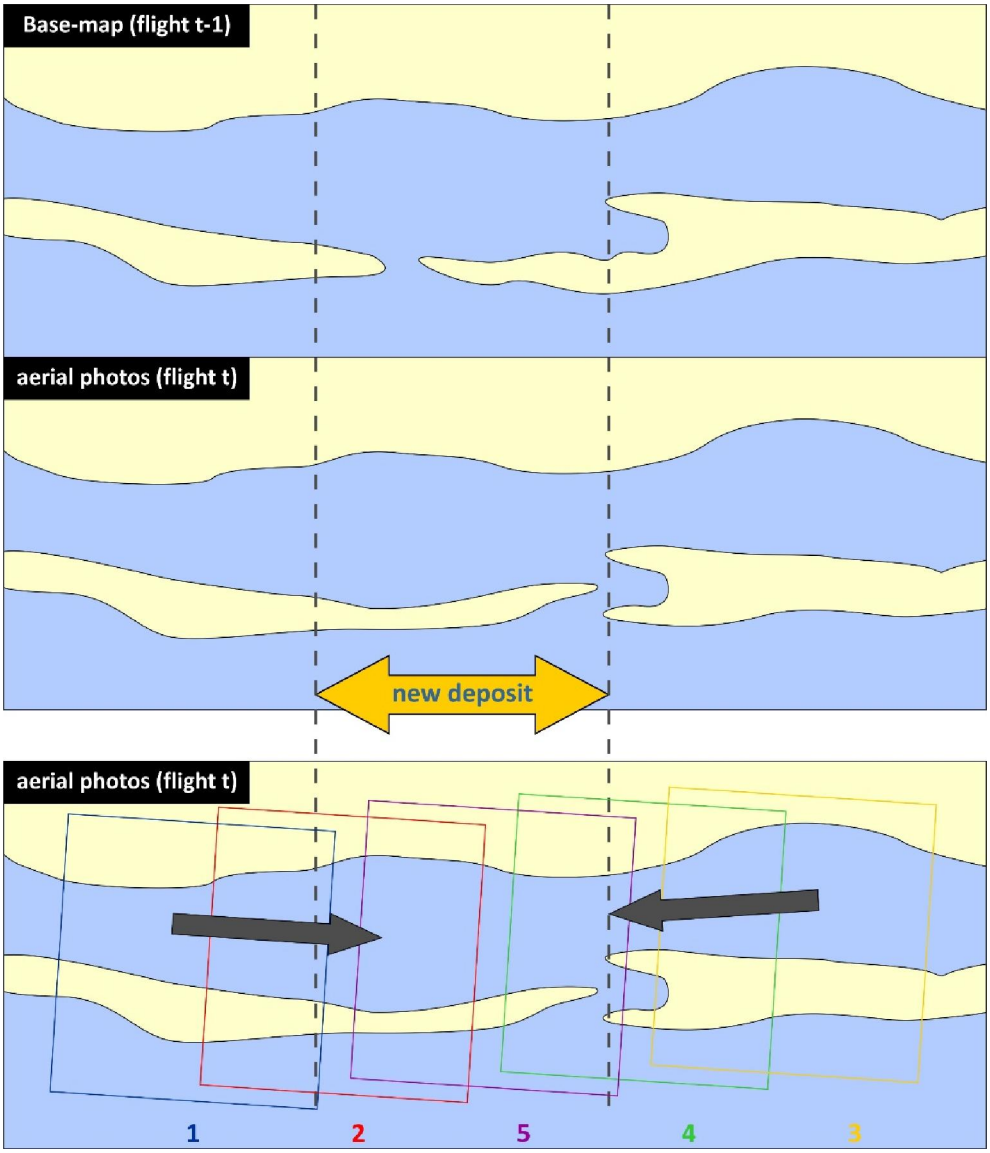

Figure 5: Schematic representation of 'problematic zone' in the vicinity of a migrating inlet and georeferencing approach used; flight t denotes the flight under georeferencing, base-map is the anterior flight (t-1), while the lower panel shows the photos as colored rectangles with the corresponding number to express georeferencing sequence and the grey arrows to show georeferencing direction. In the sketch, photos 2 and 4 are georeferenced using points on photos 1 and 3, respectively, while photo 5 (that falls on the newly deposited zone) is georeferenced using control points on photos 2 and 4.

Another investigated source of potential error was the error accumulation during the georeferencing process. This 'cumulative' error is related to the backwards in time scheme used; more specifically the use of a previously georeferenced flight as a basis for the rectification of the directly anterior flight (i.e. georeferencing 1999 using 2000 as a basis, which in turn was referenced using 2001, etc.) could potentially introduce error that can be accumulated in time. To assess this error, all georeferenced flights were compared with the 2002 orthophotography that is considered '*error-free*' and was the basis and initial point of the georeferencing process. Depending on the island and on the flight, 30 to 80 well-distributed control points were used (larger islands and/or higher resolution flights included more control points).

The results of the assessment are given in table 3 and in figure 6. It can be noted by the values that the error associated with the backwards-in-time georeferencing process does not produce accumulation of error, with the values directly comparable to the residual RMSE ones. It is noted that

for the highly dynamic Cabanas-Cacela subsystem detecting dependable points between the orthophotographs of 2002 and the aerial photographs was more difficult, the older the flight was. For flights older than 1985 it was possible to pinpoint very few common points in some of the flights (noted as highlighted values in table 3).

Table 3: 'Accumulated' RMSE for the 4 EVREST study sites and corresponding total RMSE value for all flights; n/a signifies not applicable due to flight unavailability, n/a* denotes that dependable control points were impossible to find, while values highlighted in yellow in the Cabanas-Cacela subsystem refer to values derived using a low number of points (10-14).

flight	Barreta	Culatra	Tavira	Cabanas & Cacela	Total RMSE
2000	0.77	0.84	0.77	n/a	0.79
1999	0.84	0.76	0.79	n/a	0.80
1996	0.88	0.92	0.85	1.50	1.07
1989	0.95	0.95	0.76	1.37	1.01
1989 (BW)	1.02	n/a	0.95	2.02	1.40
1986	0.89	0.72	0.79	1.80	1.07
1985	1.08	0.96	0.90	2.13	1.21
1980	0.92	1.06	0.87	6.55	1.83
1976	1.46	1.05	1.22	4.25	1.94
1972	1.05	1.05	0.83	n/a*	0.96
1969	n/a	1.00	1.06	2.52	1.31
1958	1.55	1.59	1.50	4.55	2.21
1952	1.57	1.74	1.48	n/a*	1.57
1947	2.05	1.64	2.06	n/a*	1.99

It is also important to note that for changing environments, like Cabanas and Cacela, the attempt to determine the accumulation of error cannot be performed, since the initial base map (2002 orthophotograph, in this case) lacks information regarding the geomorphological changes of the area that can only be obtained using a back-in-time process, like the one used for the georeferencing. Therefore, the error defined comparing the Cabanas-Cacela mosaics with the 2002 base map is not considered representative for flights before 1985. However, the values are included in the report as an indicator for the order of magnitude for the maximum likely accumulated error. On the other hand, highly stable environments, like Tavira and, to some extent, Barreta Island, can serve as indicators for the assessment of accumulated error in the georeferencing process.

The values presented show that the error is generally low, below 2m. This error, however, does not only reflect the error accumulation in time, but also contains the residual error values (i.e. the inherent error of the aerial photo that could not be corrected during georeferencing, see table 2). The relationship between the '*net*' accumulated RMSE (accumulated minus residual) and the flight scale is presented in figure 7. It is evident that the accumulation of error is low, ranging from 0.15 to 1.25m. For high resolution flights and disregarding the Cabanas-Cacela highly dynamic environment, for which, as analysed previously, the calculation is considered inaccurate, the accumulated error is very low, between 0.15 and 0.4m for high resolution flights and reaches 1.1m for low resolution aerial photographs. The analysis shows that the georeferencing process does not induce excessive accumulation of error and that the accuracy of the derived georeferenced rasters is uncompromised.

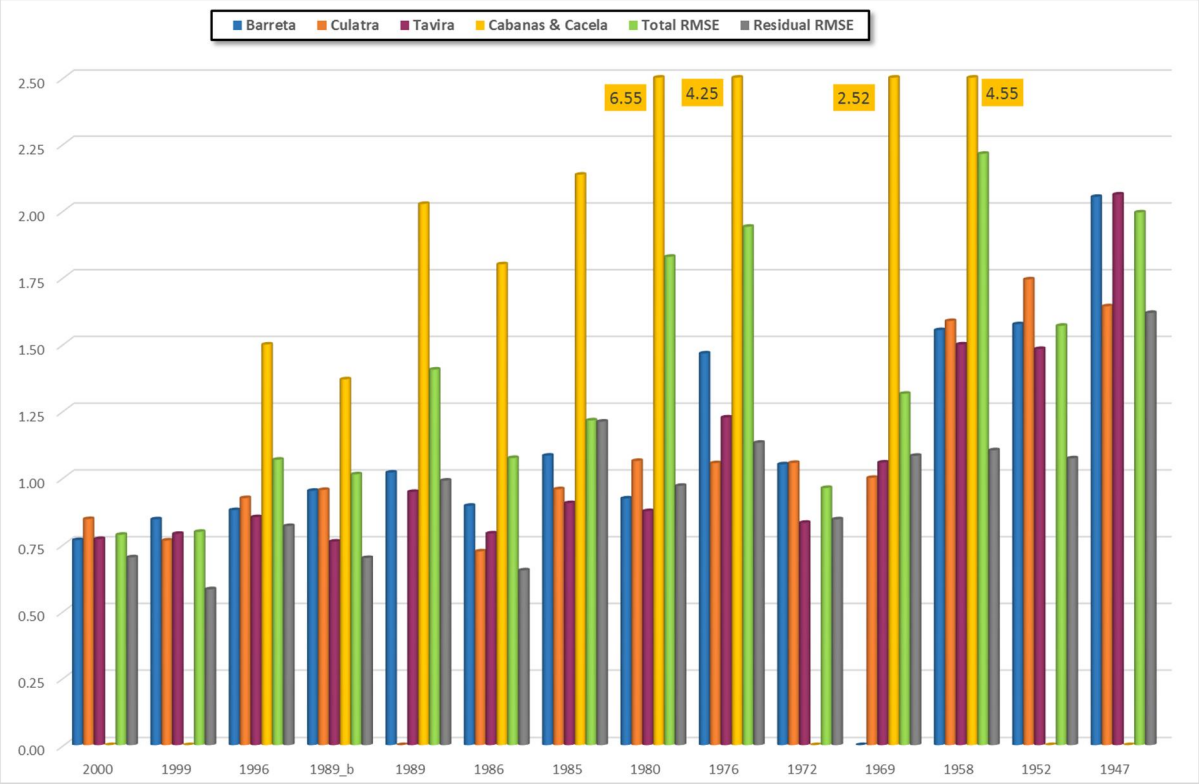

Figure 6: Bar plot of accumulated RMSE for all flights, derived comparing the georeferenced mosaics with the 2002 orthophotographs.

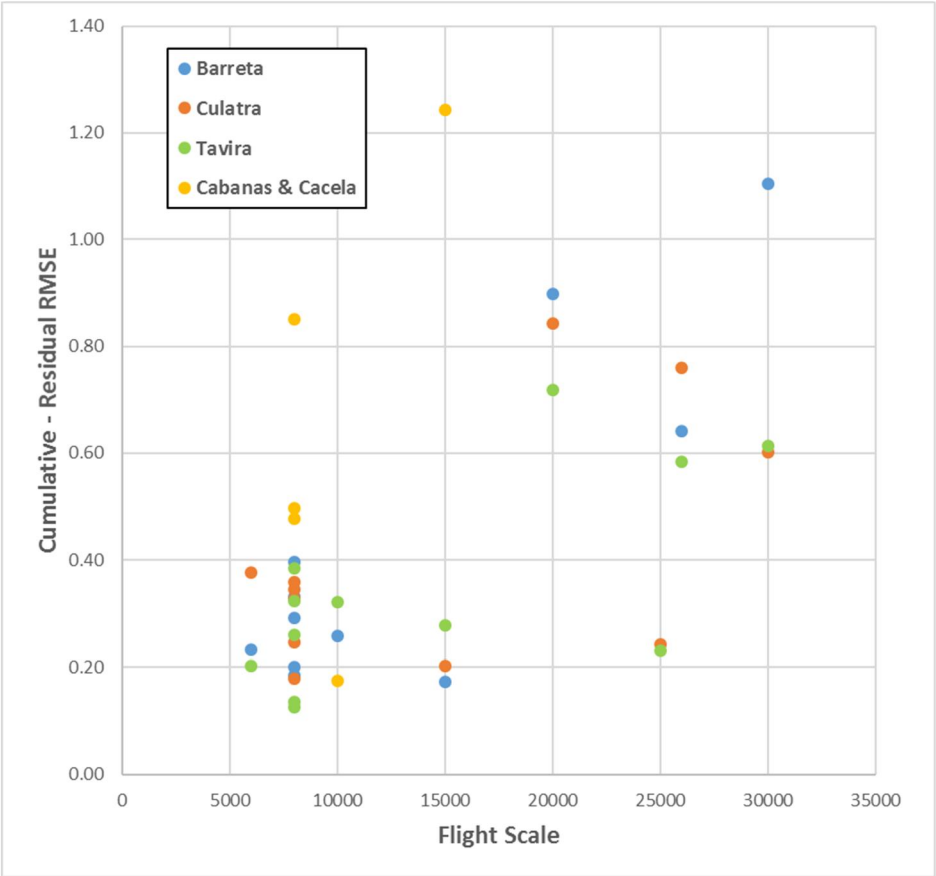

Figure 7: Comparison of subtraction remainder between accumulated and residual RMSE and scale of aerial photography. The Cabanas-Cacela mosaics older than 1985 were excluded.

3.3 Mosaicking

The individual photographs of each flight were included in one mosaicked raster dataset. In cases of aerial photographs, each raster was clipped, using polygon shapefiles in ArcMap, to remove the aerial photograph frame before introduction to the mosaic. Blending was used along the seamlines between two overlapping rasters, to ease the transition between the two images and to improve the appearance of the final mosaicked image.

Examples of the derived mosaics for the periods of 1952, 1972, 1996 and 2014 for the four EVREST study cases, namely Barreta, Culatra and Tavira islands and the Cabanas/Cacela subsystem, are given in Figure 8, Figure 9, Figure 10 and Figure 11, respectively.

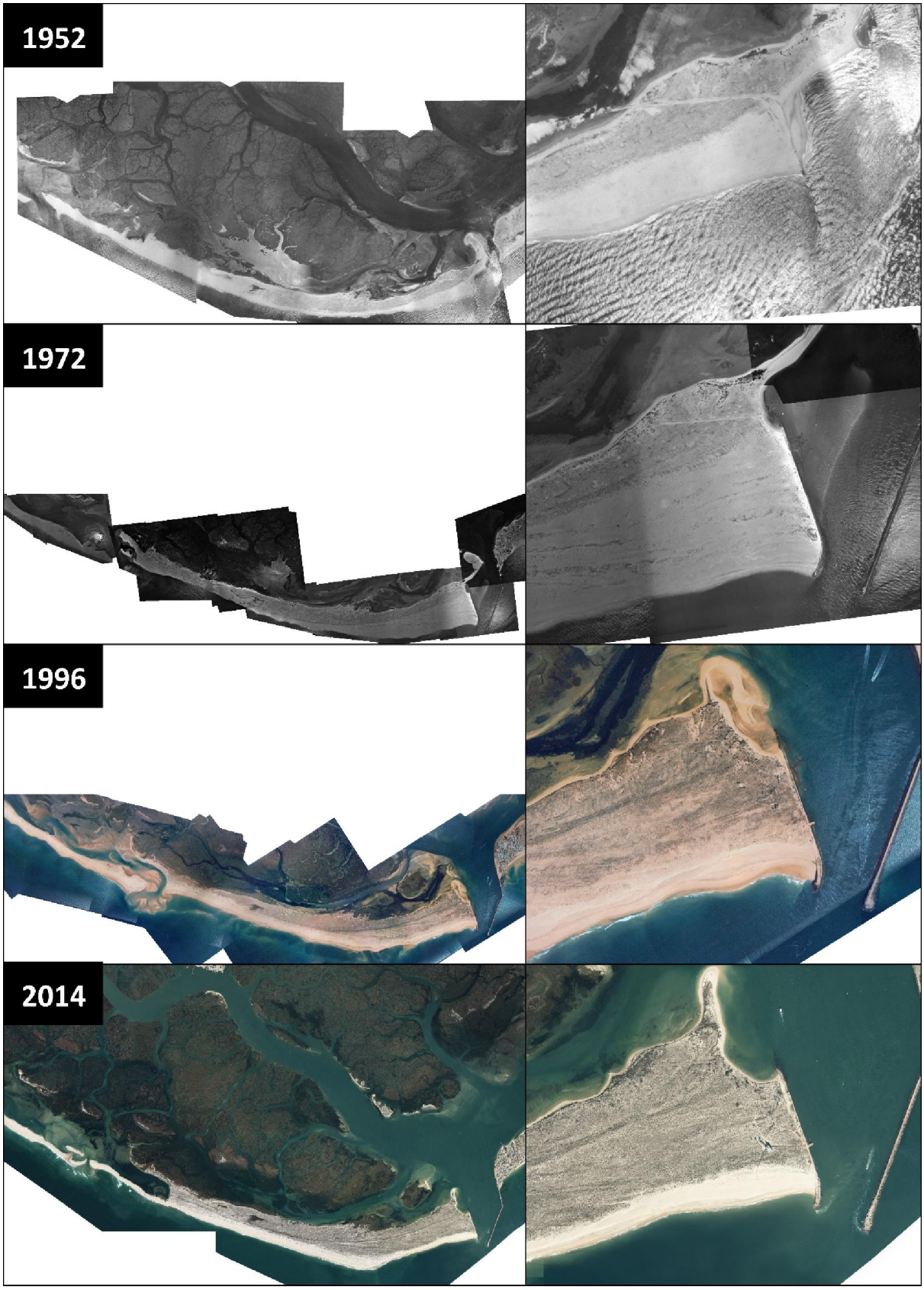

Figure 8: Barreta mosaics and related zoomed views of the eastern part of the island (EVREST study site), presented indicatively for the 1952, 1972, 1996 and 2014 datasets.

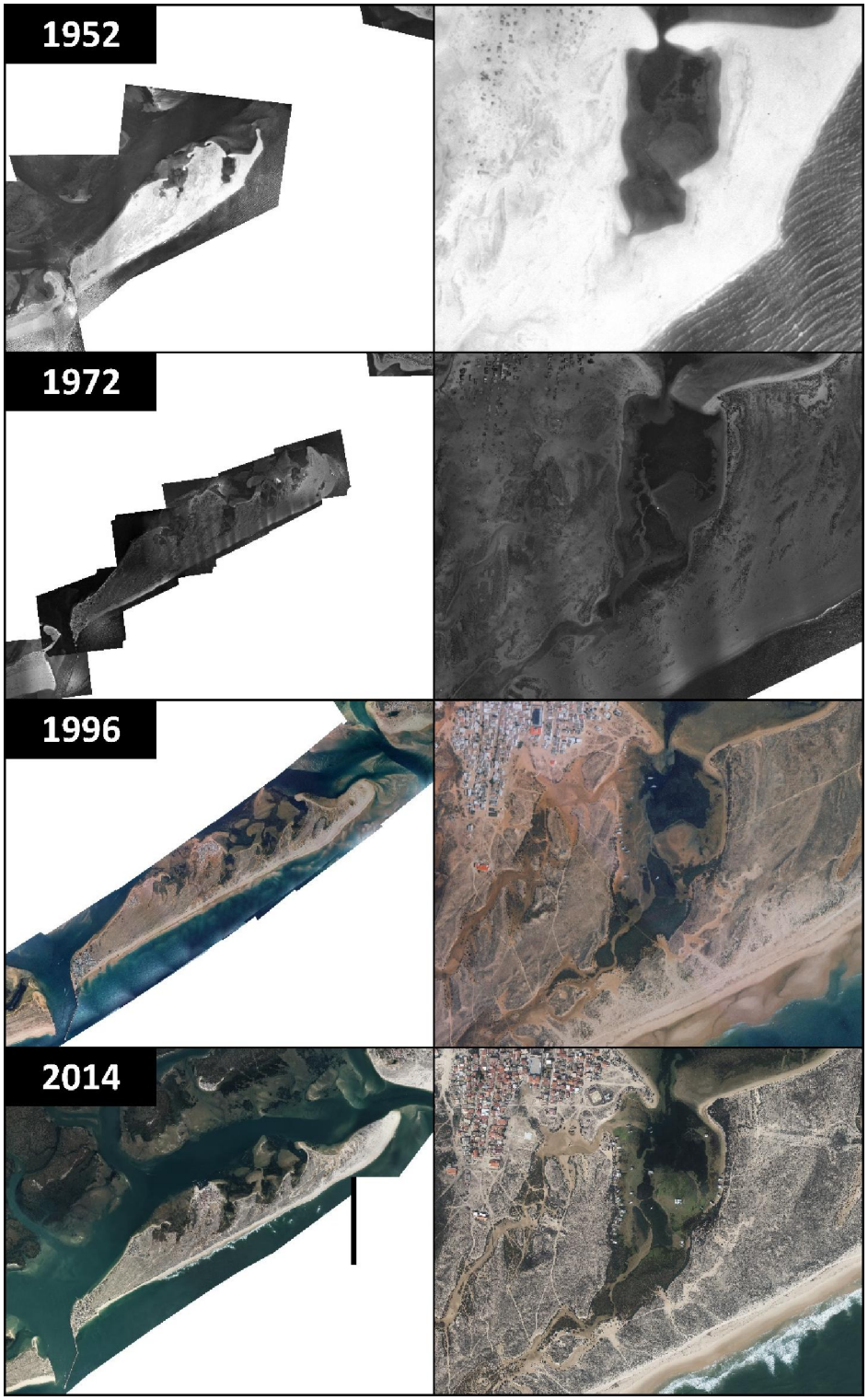

Figure 9: Culatra mosaics and related zoomed views of the embayment in the central-northern part of the island (EVREST study site), presented indicatively for the 1952, 1972, 1996 and 2014 datasets.

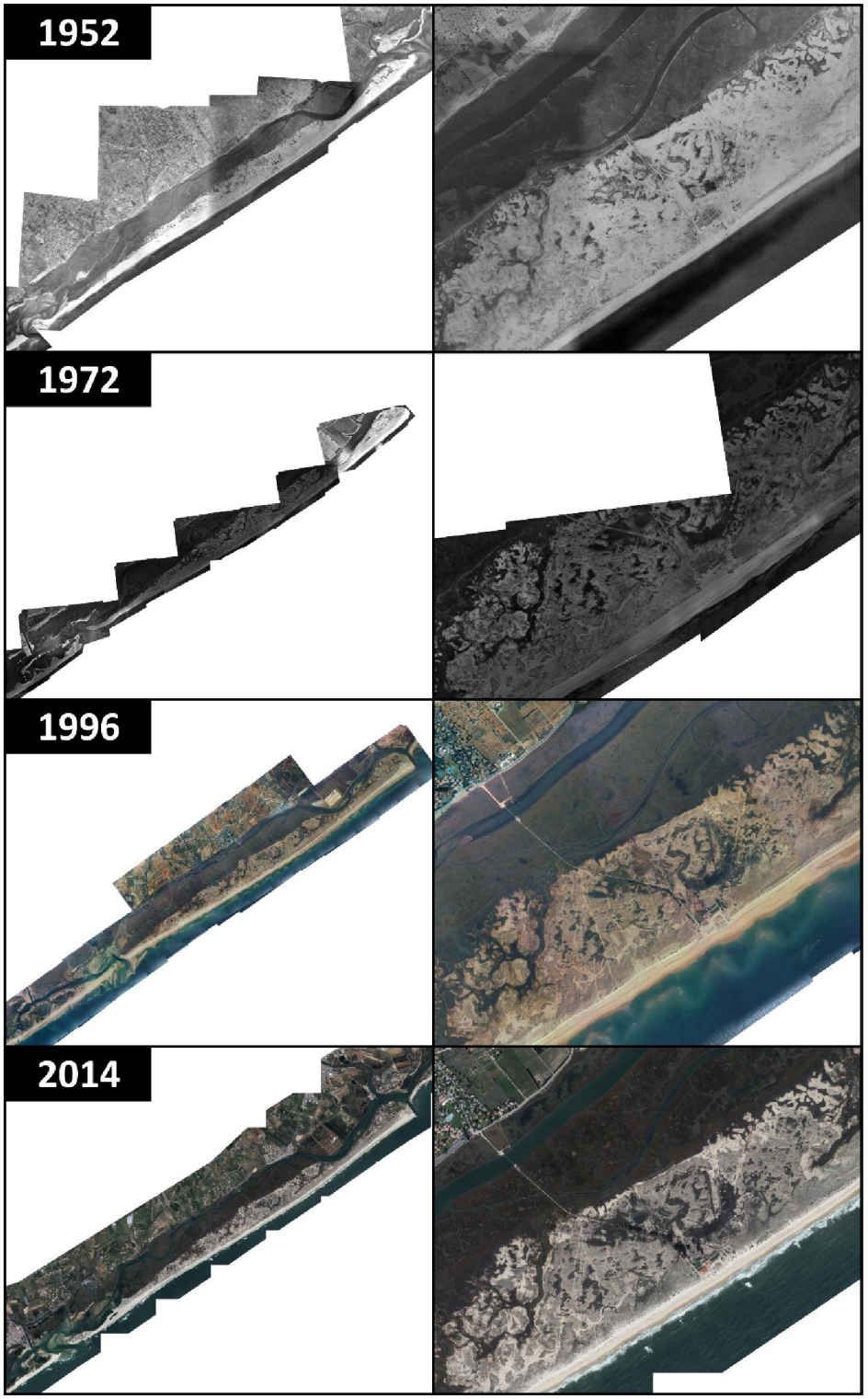

Figure 10: Tavira mosaics and related zoomed views of the central part of the island (Barril, EVREST study site), presented indicatively for the 1952, 1972, 1996 and 2014 datasets

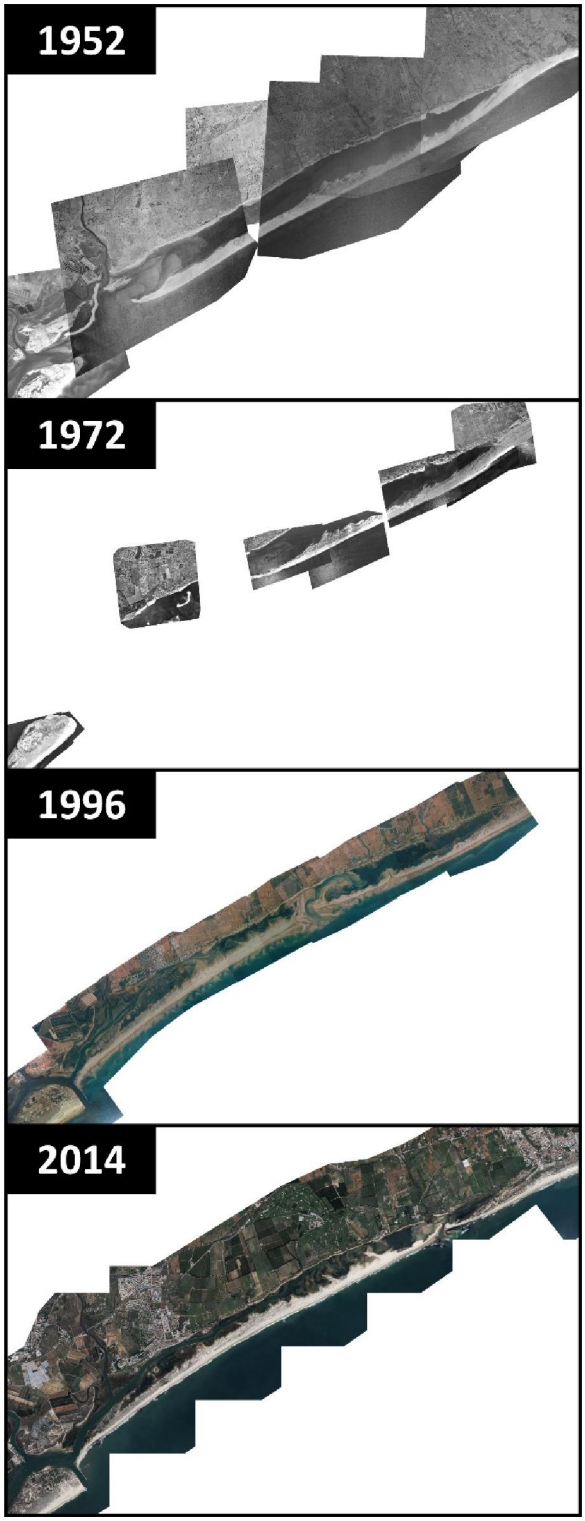

Figure 11: Cabanas and Cacela mosaics (EVREST study site), presented indicatively for the 1952, 1972, 1996 and 2014 datasets

3.4 Raster dataset metadata

The metadata provided for each mosaic dataset (Figure 12) include:

- ✓ **Title**: descriptive title for the mosaic
- ✓ **Tags**: keywords (e.g. 2001, Ria Formosa, Aerial photograph, mosaic, barrier islands)
- ✓ **Summary**: Information about the processing of the images and the funding of the EVREST project; common for all mosaic datasets.
- ✓ **Description**: list of information including 'Photograph Scale', 'Flight', 'Flight Date', 'Photo No.', 'Photo type', 'Scan Resolution', 'Film type' and 'Focal length'; depending on the flight, some information are unavailable.
- ✓ **Credits**: Acknowledgement of aerial photography copyrights and of EVREST for the GIS implementation.
- ✓ **Use limitations**: Assigned as '*Restricted Use within the EVREST Project*'.

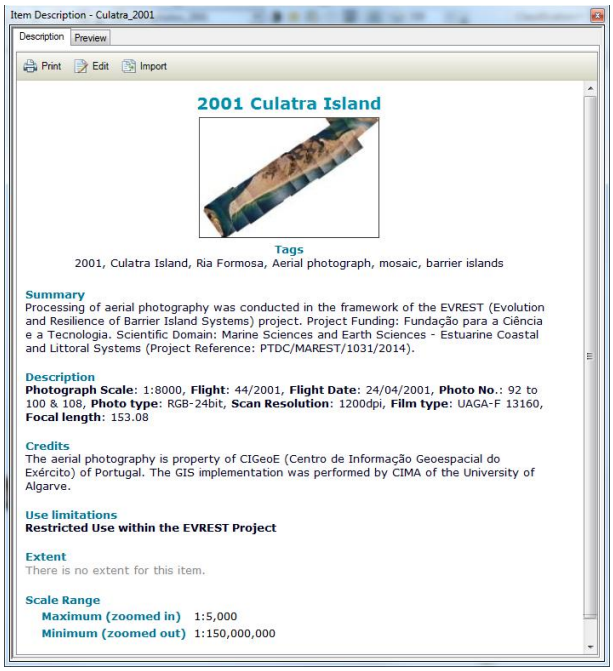

Figure 12: Example of the metadata provided for the mosaic datasets.

4. TOPOGRAPHIC DATASETS

The available LIDAR data for 2009 and 2011 were collected and processed and the final elevation maps were included in the EVREST geodatabase. An example of the elevation of 2011 is given in figure 13 for the 4 EVREST sites. Characteristics clearly visible in the elevation maps are:

a) the dune field and ridges of Barreta (Figure 13a),
b) the alternation between dune ridges and tidal channels in the central part and the curved sandy spits in the eastern part of Culatra (Figure 13b),
c) the continuous foredune and extensive backbarrier of Tavira (Figure 13c) and
d) the foredune in the western part of Cabanas and low elevations in the eastern part and in Cacela (Figure 13d).

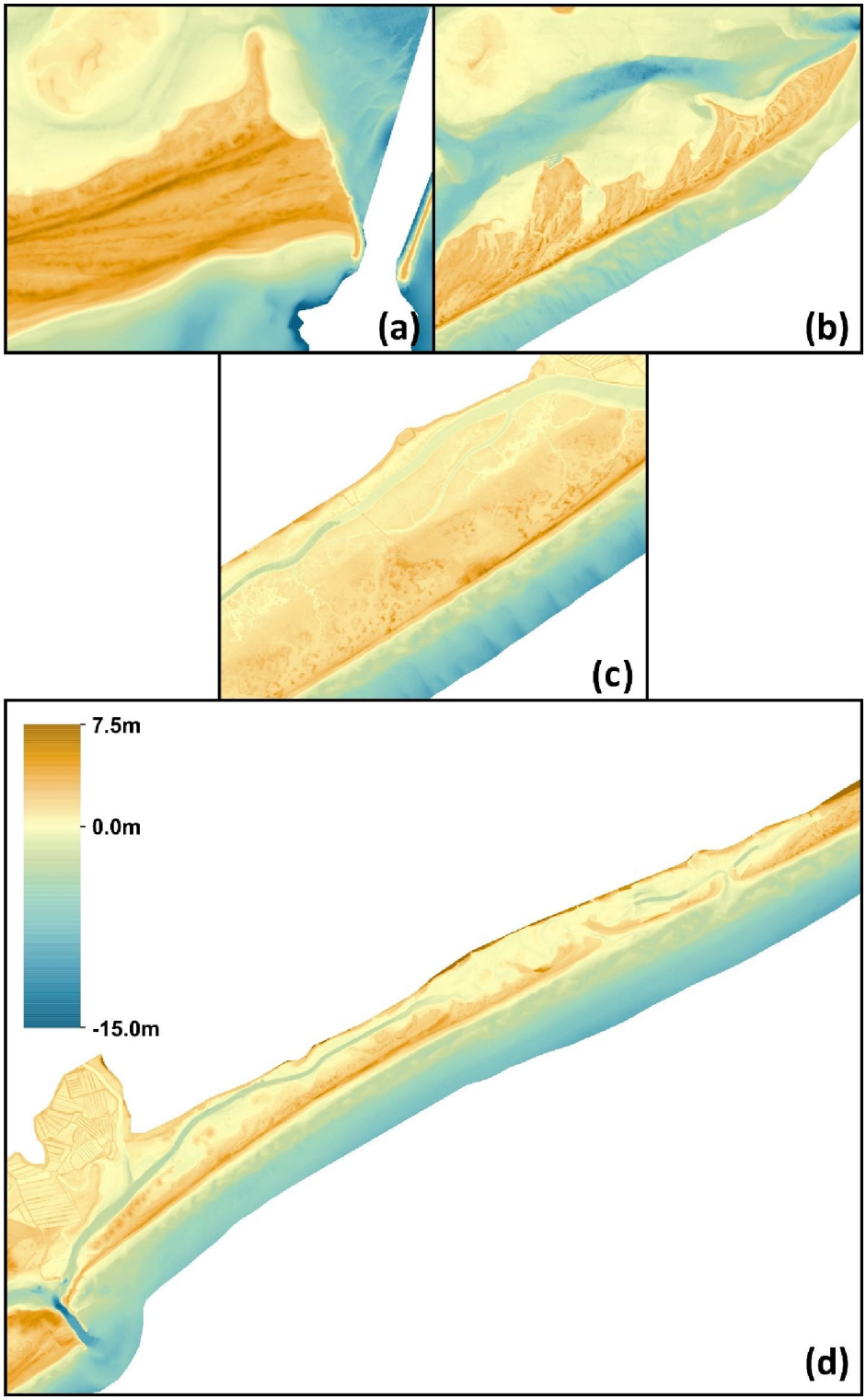

Figure 13: Elevation maps for E. Barreta (a), central-eastern Culatra (b), central Tavira (Barril; c) and Cabanas/Cacela from the 2011 LIDAR measurements; the scale bar is common for all maps.

REFERENCES

Paine, D. P., & Kiser, J. D. (2012). *Aerial Photography and Image Interpretation*. *Aerial Photography Image Interpretation: Third Edition*. Wiley. https://doi.org/10.1002/9781118110997